IV. RADIO ASTRONOMY*

Academic and Research Staff

Prof. A. H. Barrett
Prof. B. F. Burke
Prof. L. B. Lenoir
Prof. D. H. Staelin
Dr. S. H. Zisk
J. W. Barrett
Patricia P. Crowther
P. L. Seymour

Graduate Students

M. S. Ewing
N. E. Gaut
M. Melnick
J. M. Moran, Jr.
G. D. Papadopulos
E. C. Reifenstein III
A. E. E. Rogers
T. L. Wilson

A. INTERPRETATION OF SPECTRAL DATA

A microwave spectrum contains information about the temperature, pressure, and composition of the spectrum source. A basic problem in microwave observations is the optimum interpretation of observed spectra in terms of source parameters.

A good example is the problem of estimating the water-vapor profile in the terrestrial atmosphere by using observed atmospheric absorption spectra. This example is interesting because considerable use of a priori statistics must be made to obtain good performance.

A successful approach has been to assume a linear form for the optimum estimation procedure, and then to minimize the mean-square error. The estimate is

$$p^* = \underline{\underline{D}}\, d,$$

where p^* is a column matrix representing the estimated water-vapor profile, $\underline{\underline{D}}$ is the linear operator matrix, and d is the data column matrix. The optimum matrix $\underline{\underline{D}}$ is a function of the known a priori statistics and relationships governing the true water-vapor profile p and the data matrix d.

It can be shown[1] that $\underline{\underline{D}}$ is

$$\underline{\underline{D}}^t = \underline{\underline{C}}_d^{-1}\, E[d\, p^t],$$

where $\underline{\underline{C}}_d$, the correlation matrix of the data vector d, $= E[d\, d^t]$. Only second-order a priori statistics are required to minimize the mean-square error if a linear matrix estimation procedure is used. This basic method has been applied to simulated water-vapor spectral data; the results are described in Section IV-A. 1.

*This work was supported principally by the National Aeronautics and Space Administration (Grant NsG-419 and Contract NSR-22-009-120); and in part by the Joint Services Electronics Programs (U.S. Army, U.S. Navy, and U.S. Air Force, under Contract DA 28-043-AMC-02536(E).

Since microwave emission data are inherently nonlinear, it is reasonable to seek a nearly optimum nonlinear estimation procedure. A form of Baye's estimate was applied to this problem, but required inordinate amounts of computer time for any but relatively simple estimations. An extension of the linear operator technique appears more promising. Here the linear operator $\underline{\underline{D}}$ operates not only on the raw data d, but also on cross products and higher powers of the raw-data values. Thus an augmented data matrix d_a might include $(1, d_1, d_2, d_1^2, d_2^3, d_1 d_2)$, or several more elements than the original d matrix (d_1, d_2). The method for deriving the new D is essentially the same as before. The nonlinear result is

$$\underline{\underline{D}}^t = \underline{\underline{C}}_{d_a}^{-1} E[d_a p^t],$$

where d_a is the data vector augmented as illustrated above, and $\underline{\underline{C}}_{d_a}$ is the correlation matrix for the augmented data vector. The nonlinearity of the estimation procedure may be controlled by the degree to which d_a is augmented.

An interesting feature of this estimation procedure is the way that the optimum estimate requires higher order statistics in $\underline{\underline{C}}_{d_a}$ for higher order nonlinearities in the estimation procedure. If d_a includes elements like $d_i d_j$, then $\underline{\underline{C}}_{d_a}$ may include elements like $E[d_i d_j d_k d_l]$. This nonlinear estimation procedure appears to be practical for many problems involving interpretation of spectra, and could probably be applied in many other areas.

D. H. Staelin

References

1. C. D. Rogers, "Satellite Infrared Radiometer, A Discussion of Inversion Methods," Memorandum No. 66.13, Oxford University, 1966.

1. RESULTS OBTAINED FROM THE INVERSION OF SIMULATED ATMOSPHERIC WATER-VAPOR SPECTRA

An optimum linear estimator for inverting spectral data has been outlined in Section IV-A. Its form is

$$p^* = \underline{\underline{D}}\, d,$$

in which p^* is the estimated column vector for the parameter of interest; d, the column vector representing spectral and other, if any, related data; and $\underline{\underline{D}}$, the linear operator matrix relating p^* and d.

Minimizing the mean-square error between p^* and the true profile p leads to an expression from which $\underline{\underline{D}}$ may be computed. In the vertical profile of atmospheric water vapor, for which the water-vapor density is the parameter of interest, it can be shown that this expression becomes

$$\underline{\underline{D}}^t = \underline{\underline{C}}_d^{-1} E[d\ \rho^t] = [\underline{\underline{C}}_o + \underline{\underline{C}}_n]^{-1}\ \underline{\underline{W}}\ \underline{\underline{C}}\rho.$$

Here, $\underline{\underline{W}}$ is the modified weighting-function matrix for atmospheric absorption, and $\underline{\underline{C}}_o$ is the noiseless data correlation matrix defined by

$$\underline{\underline{C}}_o = E\left[d_o\ d_o^t\right] = \underline{\underline{W}}\ \underline{\underline{C}}\rho\ \underline{\underline{W}}^t,$$

in which $\underline{\underline{C}}\rho$ is the atmospheric water-vapor correlation matrix given by

$$\underline{\underline{C}}\rho = E[\rho\ \rho^t],$$

and $\underline{\underline{C}}_n$ is the noise correlation matrix defined by

$$\underline{\underline{C}}_n = E[n\ n^t].$$

Preliminary inversions have been completed. We have used as input computed absorption spectra from each radiosonde at the following frequencies: 21.9, 23.5, and 29.45 GHz. As an additional data point, we have used the water vapor density at

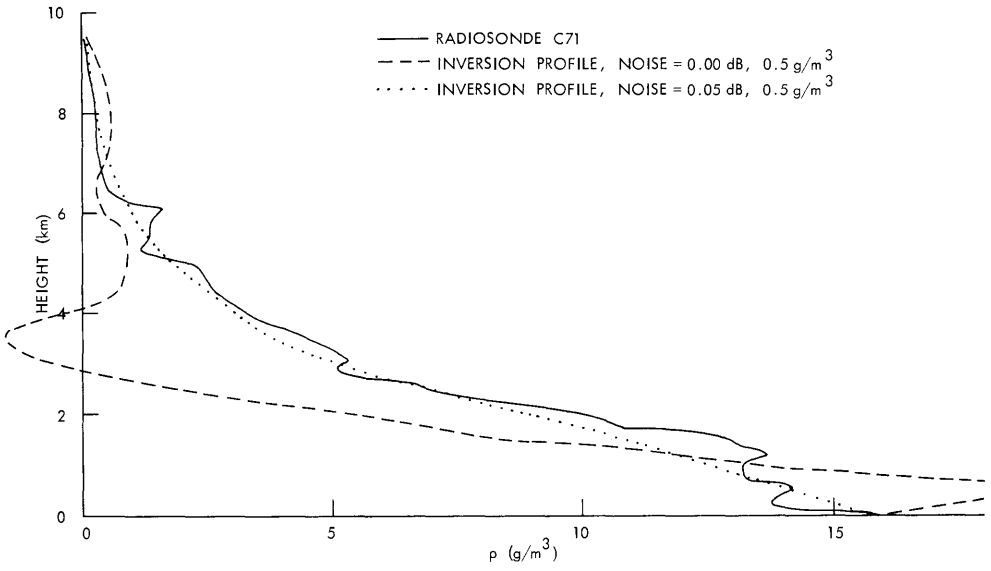

Fig. IV-1. Radiosonde C71 results.

the surface. Two radiosondes with their corresponding inversion profiles are illustrated in Figs. IV-1 and IV-2.

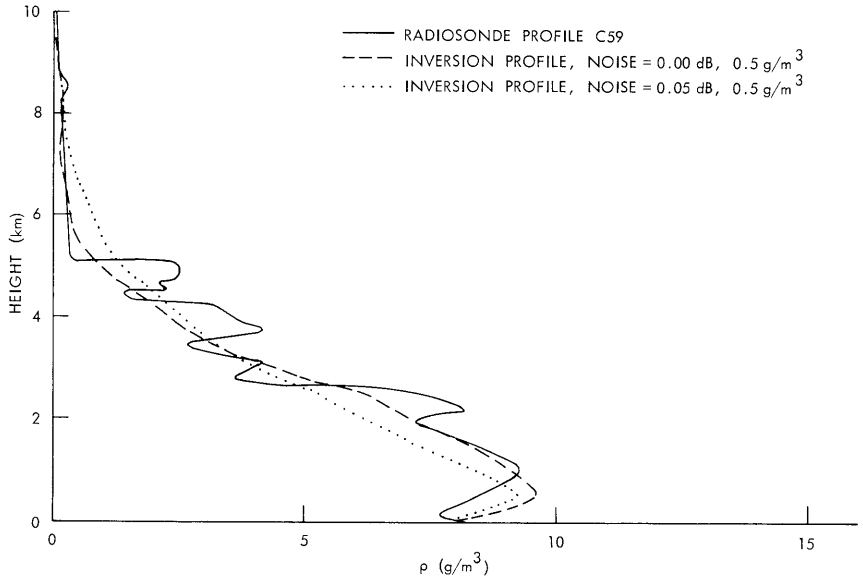

Fig. IV-2. Radiosonde C59 results.

Figure IV-1 best ilustrates the effect of noise on inversion. The solid profile is the water-vapor density as recorded by radiosonde C71, which was launched 10 August 1965. The dashed profile represents the inversion when there is assumed to be no noise in the spectral data, but that surface water-vapor density is uncertain to the extent of 0.5 g/m^3. A grossly unstable inversion results. When the spectral data are assumed to have an rms error of 0.05 db, the inversion is stabilized and represents the true profile quite well. The zero noise case, however, represents an integrated water vapor that differs only -0.2% from the integrated water vapor derived from the radiosonde, whereas the noise case differs by -2.8%.

This latter effect is a general feature of the inversion scheme. Noise stabilizes the solution but also drives the inversion toward the mean profile as defined by the a priori statistics. In this case, the mean represents less integrated water vapor than the true profile, and therefore the estimated total water vapor is driven toward smaller values in the noise case.

Figure IV-2 is included to show that strong inversions of moisture near the surface of the earth can be indicated, if not faithfully reproduced, by this scheme. The radiosonde illustrated here was taken 14 July 1965. The dashed profile is the noiseless case, and, for this radiosonde, is a better representation of the true

profile than the noise case. The other oscillations of the true profile will not be recoverable by using the present data input, unless they appear in the a priori statistics. The integrated water vapor for the noiseless case differs from the true value by -1.3%. The noisy inversion differs by -4.3%.

Figure IV-3 is a histogram showing the distribution of percentage errors between

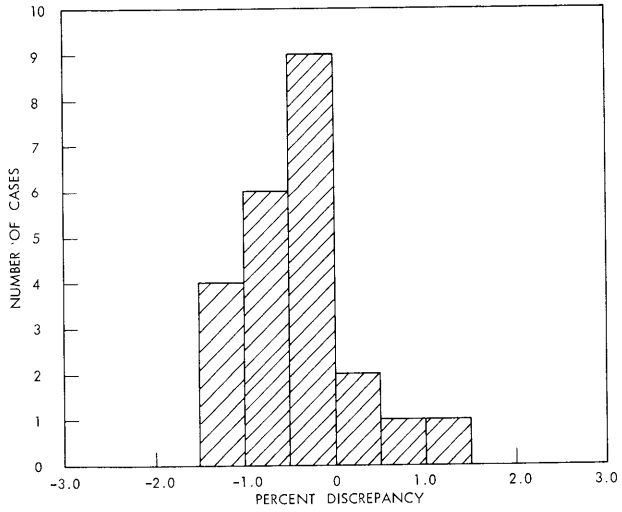

Fig. IV-3. Integrated water vapor percentage of errors.

the integrated water vapor as computed from the inversion profiles and the corresponding radiosonde profiles. The noise for these inversions was taken to be 0.005 db and 0.5 g/m^3. The errors are skewed toward negative values, with the mean near -0.5%

Further analysis using simulated data will be conducted to understand completely the roles of noise, sampling intervals, and the a priori statistics. An analysis with observed atmospheric absorption spectra is being prepared.

N. E. Gaut, A. H. Barrett, D. H. Staelin

2. MICROWAVE DIELECTRIC CONSTANT AND EMISSIVITY OF A SOLUTION APPROXIMATING SEA WATER

For staellite-borne microwave radiometers looking at the Earth, much of the background radiation will originate from sea water at various temperatures. In order to better understand this source of radiation, the complex dielectric constant and emissivity for sea water as a function of wavelength, temperature, and angle of incidence was studied. The real part of the dielectric constant, and that portion of the imaginary part

which is due to losses from the oscillations of polar molecules, came from work on 0.66 normal aqueous solutions of NaCl.[1] That portion of the imaginary part of the dielectric constant which is due to ohmic losses was computed from tables of the DC conductivity of sea water.[2] The use of the DC conductivity for high-frequency work appears to be justified from the measurements made on the salt solutions referred to above.

Details of the real part of the dielectric constant for the salt solution at various temperatures and over the wavelength interval 0.5-22 cm are presented in Fig. IV-4.

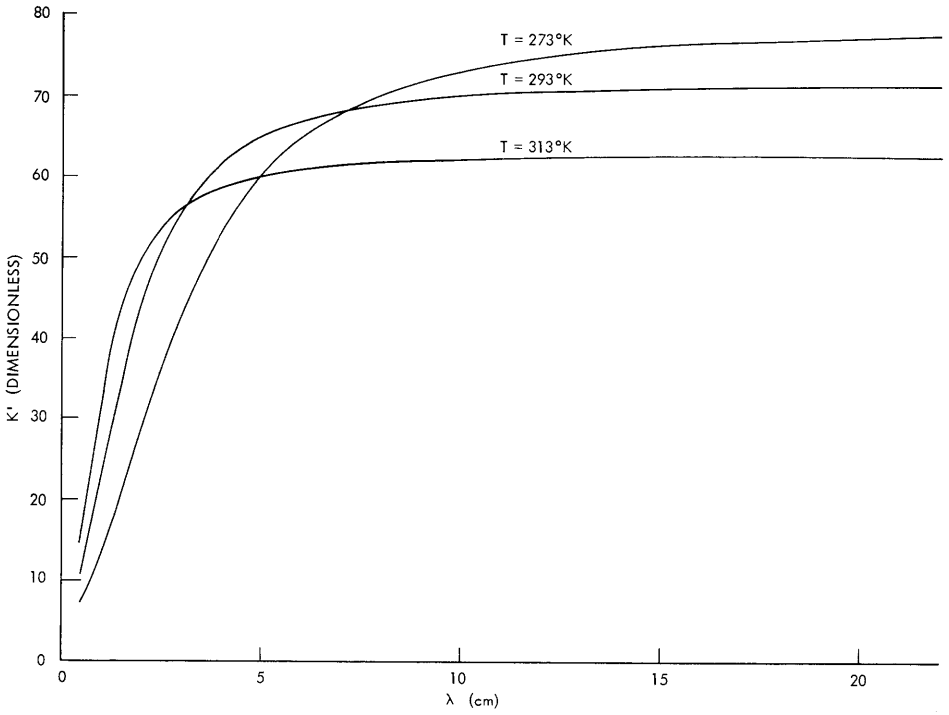

Fig. IV-4. Sea water (0.66N NaCl). Real part of the dielectric constant (K') vs wavelength.

It is important to notice the reversal of the temperature effect between the shortest and longest wavelengths depicted, with an anomalous region in the vicinity of 3-5 cm.

The complex part of the dielectric constant for the solution is shown in Fig. IV-5, again as a function of temperature and wavelength. It can be seen that the sense of the temperature effect is similar at the shortest and longest wavelengths; however, between approximately 2 cm and 6 cm, the temperature effect is reversed. This is understandable because the dielectric losses predominate in this region, and their temperature dependence completely reverses near 2 cm. Beyond 9 cm, the conduction losses dominate and the temperature effect is restored to its short-wavelength sense.

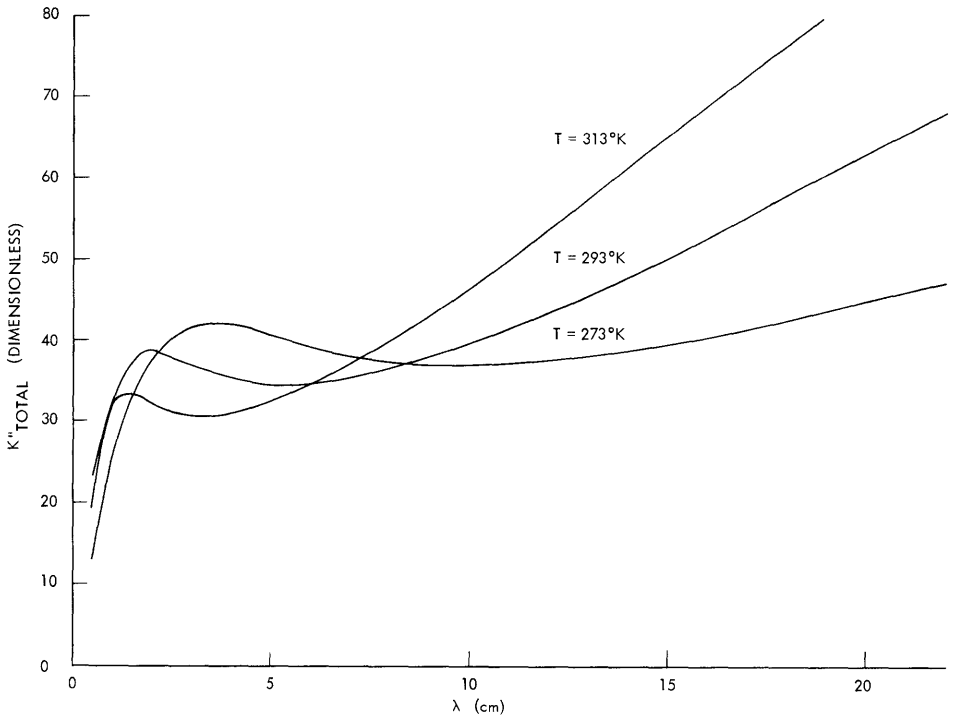

Fig. IV-5. Sea water. Imaginary part of the dielectric constant (K''_{total}) vs wavelength.

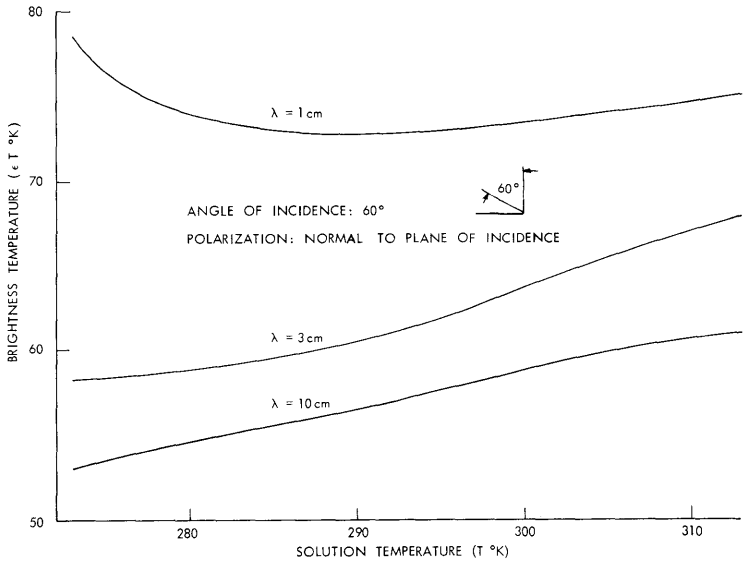

Fig. IV-6. Sea Water. Brightness temperature vs solution temperature.

Anomalous transition regions occur between approximately 0.8 cm and 2 cm, and between approximately 6 cm and 9 cm.

Figure IV-6 incorporates information from Figs. IV-4 and IV-5, and represents the brightness temperature as a function of thermometric temperature of the solution at wavelengths of 1, 3, and 10 cm, for an angle of incidence of 60° and for polarization normal to the plane of incidence. This figure is a corrected version of Fig. II-1 in Quarterly Progress Report No. 81 (page 11). The computations for that figure did not include losses attributable to conduction currents. The essential features of the original figure are retained in Fig. IV-6.

N. E. Gaut

References

1. J. B. Hasted, D. M. Ritson, and C. H. Collie, J. Chem. Phys. 16, 1 (1948).
2. American Institute of Physics Handbook, 2d edition, 1963.

B. HYDROGEN RECOMBINATION LINE OBSERVATIONS

The first observational phase of a program to make a survey of radial velocities of H II regions throughout the galaxy has been completed. The 140-ft telescope and 6-cm front end of the National Radio Astronomy Observatory was used, together with the Harvard multichannel spectral analyzer, to observe the 109α hydrogen recombination line. The system temperature (70°K) permits observation of lines as weak as 0.05°K in 30 minutes, with 100-kHz resolution. The recombination lines have been observed in 52 of the H II regions that have been reduced thus far, and several more identifications are expected when data analysis has been completed. There are several high-velocity regions among those observed, the highest velocity observed being 119 km/sec.

The general survey will be used to construct a dynamical model of the galaxy, analogous to the well-known 21-cm model of the Leiden and Sydney groups, which shows the distribution of neutral hydrogen in the galaxy. The new model will show the distribution of O-associations which form the H II regions, and hence should be closely related to optically derived galactic models. From the observations, a rotation law should eventually be derived, although further observations will be required to improve our statistics.

The region of the galactic center has also been examined closely, and we have been able to correct the early observations of Hoglund and Mezger, who incorrectly attributed the lines from the sources G 0.5, -0.0 and G 0.7, -0.1 to G 0.2, 0.0, and G 0.5, -0.5, respectively. We have been unable to detect a line of normal linewidth (30 km/sec, or so) in G 0.0, 0.0 and G 0.2, 0.0, but the existence of a broad feature in these sources cannot

be excluded.

Cygnus X is an especially interesting region, and all of the major sources identified by Downes and Rinehart have been observed. Several of these sources, although they are believed to be thermal, show no line of the expected intensity, and the possibility that a number of the "thermal" sources are really old supernovae remnants with rather flat spectra is now being examined.

B. F. Burke, T. L. Wilson, E. C. Reifenstein III

C. OBSERVATIONS OF OH EMISSION

Observation of the ground-state emission lines of $O^{16}H^{1}$ at 18 cm near galactic H II regions have shown that the apparent diameters of the emitting regions are very small.[1-3] The sources associated with individual spectral features in W3, W49, and W24 (Sgr B_2) were all unresolved by an interferometer having a baseline of 3800 λ. In particular, an upper limit of 20" of arc was found for the size of the 4 strongest features in W3. All features were reported to be at the same position within 3" of arc near the edge of the optical nebulosity of the H II region. The size limits imply brightness temperatures in excess of 10^6 °K, although the linewidths of the features were characteristic of kinetic temperatures of approximately 100°K. All emission sources were polarized and exhibited anomalous multiplet intensity ratios. A quantitative explanation for the emission mechanism has not been found.

Increased angular resolution has been obtained with a new interferometer, by using the 84-ft Millstone antenna at Lincoldn Laboratory and the 60-ft antenna at the Agassiz Field Station of Harvard College Observatory. The baseline was 74,400 λ at 18 cm along a bearing of 24° East of North, which gives a minimum fringe spacing of approximately 3" of arc. An effective system temperature of 300°K was achieved with the Agassiz maser amplifier and a tunnel-diode amplifier at the Millstone antenna. The strongest spectral feature of W3 yielded a signal-to-noise ratio of 8:1, with only 1 minute of integration. The measurements were made with linearly or circularly polarized feeds on the Millstone antenna and a linearly polarized feed on the Agassiz antenna. The polarizations were almost always nonorthogonal, since the Millstone antenna is altazimuth-mounted and the Agassiz antenna is polar-mounted.

The two stations were connected by a 7-GHz microwave link which carried a 5-MHz local-oscillator reference signal and an IF channel having a 400-kHz bandwidth from the Agassiz site to the Millstone site. The IF signals were effectively crosscorrelated by the use of a phase-switching technique and a digital autocorrelator. A computer was programmed to obtain the fringe amplitude and phase information as a function of frequency from the correlation functions. The phase stability of the system permitted integration periods of 1 minute. Longer integration periods were achieved by averaging

vectorially the fringe amplitude and phase for each frequency, by using the phase of the strongest feature as a reference phase. Hence, relative fringe phases among the various spectral components were obtained.

Observations were made of the 1665-MHz transition in source W3, during November 1966 and January 1967. The fringe amplitudes of the features at -43.7 km/sec and -46.5 km/sec were found to be unity over a local hour-angle coverage of 16 hours. The feature at -45.1 km/sec also gave unity fringe amplitude when observed with right-circular polarization. The normalizations were made by using single-antenna flux measurements of the source. Under the assumption of uniformly bright circular disks as a source model, the features were found to be smaller than 2" of arc in diameter. Recent observations by Davies, Rowson, Booth, Cooper, Gent, Adgie, Crowther[4] have reduced these size limits to 0.1", or smaller, for the individual features in this region.

The right-elliptical and left-elliptical features at -45.1 and -45.5 km/sec, respectively, when observed, were blended with linear polarization. The fringe amplitude function of this superposition did not follow the local hour-angle dependence expected for a single point source with the polarization parameters given by Meeks, Ball, Carter, and Ingalls.[5] A model that fits the observations can be constructed of two components separated approximately 1" of arc. Further observations are planned with improved sensitivity and with orthogonally polarized feeds, which should yield further information about the angular distributions of polarization and brightness.

The relative fringe phases between the strong features are shown in Fig. IV-7.

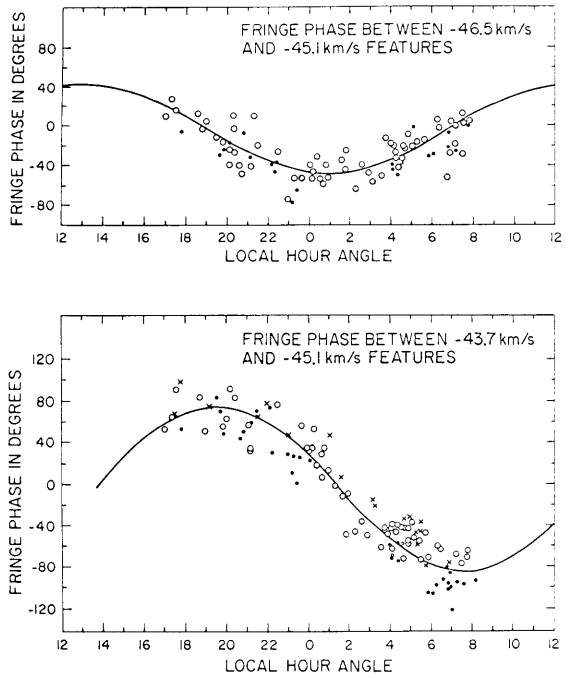

Fig. IV-7

Fringe phase between -43.7 and -45.1 km/sec features and between -46.5 and -45.1 km/sec features as a function of Local Hour Angle for the 1665-MHz OH transition in W3. Each data point represents 10 minutes of integration. Horizontal, vertical, and circular polarization points are represented by the symbols o, •, and x. The velocities are based on a rest frequency of 1665.401 MHz for the $F = 1 \rightarrow F = 1$ transition of the $^2\pi_{3/2}$ state.

The expected phase difference, $\Delta\phi$, for point sources separated by $\Delta\alpha$ in Right Ascension and by $\Delta\delta$ in Declination is given by

$$\Delta\alpha = \omega_o \frac{D}{C}\{[\sin\delta_B \cos\delta_S - \cos\delta_B \sin\delta_S \cos(L_S - L_B)]\,\Delta\delta + [\cos\delta_B \cos\delta_S \sin(L_S - L_B)]\Delta\alpha\},$$

where δ_B, L_B, δ_S are the Declination and Local Hour Angle of the baseline and the source, respectively, $\omega_o/2\pi$ is the frequency, D is the baseline length, and c is the

Table IV-1. Sizes and separations of features in 1665-MHz OH spectra of W3.

Feature	Polarization	Fringe Amplitude	Size	$\Delta\alpha$	$\Delta\delta$
-43.7 km/s	R.E.	1 ± .2	2"	$.12^s$ ± .04	-.15" ± .3
-45.1	R.E.	1 ± .1	1"	0	0
-46.5	L.	1 ± .2	2"	$-.01^s$ ± .04	-.45" ± .3

The quoted uncertainties represent two standard deviations for the parameter estimates made from the data in Fig. IV-7.

velocity of light. The data were found to follow this relation and yielded the position offsets listed in Table IV-1, with the -45.1 km/sec feature used as a reference position. The position errors were limited by the noise level in the relative phase measurements. A sketch of the source model is given in Fig. IV-8. Solid lines indicate

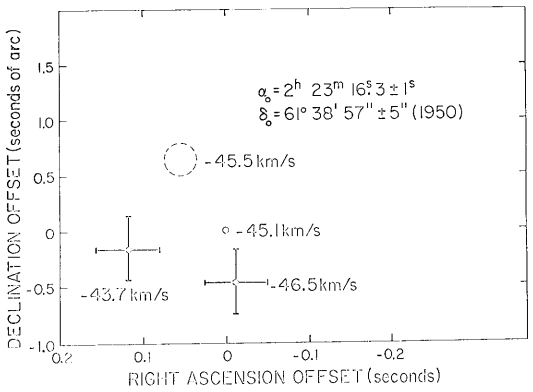

Fig. IV-8. Map of the relative positions of the centers of the 4 strongest features in the W3 OH source. The coordinates are the absolute position derived from the short baseline interferometer measurements of Rogers, Moran, and Crowther.[2]

the positions for the -43.7 and -46.5 km/sec features, while the position for the -45.5 km/sec feature is model-dependent, and hence is shown by dotted lines.

An angular size of 2" of arc corresponds to a linear dimension of 3400 astronomical

units, or 0.016 parsecs if the distance to W3 is taken to be 1700 parsecs. This implies that the radio brightness temperatures of these regions must be greater than 10^9 °K from our measurements or 10^{11} °K from the recent results of Davies and co-workers.[4] The angular size determined by these observations may be an apparent size only. If a coherent phenomenon such as maser action is occurring, the dimension of the region can be much larger than the size inferred from our measurements.

J. M. Moran, Jr., A. H. Barrett, A. E. E. Rogers, B. F. Burke

References

1. A. E. E. Rogers, J. M. Moran, P. P. Crowther, B. F. Burke, M. L. Meeks, J. A. Ball, and G. M. Hyde, Astrophys. J. 147, 369-377 (1967).
2. A. E. E. Rogers, J. M. Moran, and P. P. Crowther, Phys. Rev. Letters 17, 450-452 (1966).
3. D. D. Cudaback, R. B. Read, and G. W. Rougoor, Phys. Rev. Letters 17, 452 (1966).
4. R. D. Davies, B. Rowson, R. S. Booth, A. J. Cooper, H. Gent, R. L. Adgie, and J. H. Crowther (to appear in Nature).
5. M. L. Meeks, J. A. Ball, J. C. Carter, and R. P. Ingalls, Science 153, 978 (1966).